Lamb dip CRDS of highly saturated transitions of water near 1.4 μm

S. Kassi,[1] T. Stoltmann,[1,2] M. Casado,[1,2] M. Daëron,[2] and A. Campargue[1,a)]
[1]*Université Grenoble Alpes, CNRS, LIPhy, 38000 Grenoble, France*
[2]*LSCE-IPSL, UMR 8212, CEA-CNRS-UVSQ-UPS, Gif-sur-Yvette, France*

(Received 28 October 2017; accepted 15 January 2018; published online 2 February 2018)

Doppler-free saturated-absorption Lamb dips were measured at sub-Pa pressures on rovibrational lines of $H_2{}^{16}O$ near 7180 cm^{-1}, using optical feedback frequency stabilized cavity ring-down spectroscopy. The saturation of the considered lines is so high that at the early stage of the ring down, the cavity loss rate remains unaffected by the absorption. By referencing the laser source to an optical frequency comb, transition frequencies are determined down to 100 Hz precision and kHz accuracy. The developed setup allows resolving highly *K*-type blended doublets separated by about 10 MHz (to be compared to a HWHM Doppler width on the order of 300 MHz). A comparison with the most recent spectroscopic databases is discussed. The determined *K*-type splittings are found to be very well predicted by the most recent variational calculations. *Published by AIP Publishing.* https://doi.org/10.1063/1.5010957

I. INTRODUCTION

The accuracy of the determination of the center of an absorption line depends on the accuracy of the calibration of the frequency axis and on the precision of the line center determination. In recent years, the measurement of absolute frequencies has greatly benefited of the advent of self-referenced optical frequency combs (OFCs).[1] For instance, frequency-stabilized cavity ring-down spectroscopy (CRDS) referenced to a Cs atomic clock through an optical frequency comb was applied to the measurement of $^{12}C^{16}O_2$ transition frequencies with combined standard uncertainties of a few tens kHz over the large 1.6–7.8 μm range.[2] Recently, Bielska *et al.* measured the frequency of a B-band transition of oxygen near 690 nm with kHz level of accuracy by using a Pound-Drever-Hall-locked frequency-stabilized cavity ring-down spectrometer referenced to an ^{88}Sr optical atomic clock *via* an optical frequency comb.[3] These state-of-the-art results are limited to a few very well isolated spectral lines recorded with very high signal to noise ratio through dedicated experimental setups. In general, due to the Doppler broadening in the near-infrared amounting to several hundred MHz at room temperature, typical line center accuracy in the Doppler regime hardly reaches the MHz (3×10^{-5} cm^{-1}) level.[4–6] This is typically the case for the comb-assisted cavity ring-down spectroscopy (CA-CRDS) approach which combines absolute-frequency and high sensitivity.[7] Our CA-CRDS setup[8] measures "on the fly" the beat note frequency between one of the modes of the frequency comb and a small part of the light emitted by a Distributed Feedback (DFB) laser diode used as a source of the cavity ring-down spectrometer. CA-CRDS has provided slightly sub-MHz accuracy of CO, D_2, and water line centers in routine over broad spectral regions between 1.7 and 1.3 μm.[8–10]

Saturation spectroscopy is a powerful method to overcome limitations imposed by Doppler broadening.[11] Saturated transitions exhibit a Lamb dip at their line center with a width several orders of magnitude narrower than the Doppler broadening. The increased intracavity power provided by cavity-enhanced absorption spectroscopy techniques makes them a very well-suited method to saturate transitions in different spectral ranges from the infrared to the visible (see, e.g., Refs. 12–15). For instance, Lisak and Hodges measured Lamb dips of four closely spaced rovibrational water vapor absorption transitions near 7100 cm^{-1} using frequency-stabilized CRDS.[16] In the absence of an OFC, absolute transition frequencies were not determined but a 50 kHz resolution was achieved and relative transition frequencies were determined with an uncertainty better than 400 kHz. Galzerano *et al.* used the Lamb dip of an $H_2{}^{17}O$ transition near 1.384 μm to frequency stabilize an external-cavity diode laser.[17] The same group reported a Lamb dip center frequency of a $H_2{}^{18}O$ transition near 1.38 μm with 10 kHz accuracy by OFC-assisted cavity-enhanced saturated absorption spectroscopy.[18] This transition, which is selected to obtain an accurate spectroscopic determination of the Boltzmann constant, is very strong (line intensity on the order of 2×10^{-20} cm/molecule). Recently, Burkart *et al.* used an optical feedback frequency-stabilized cavity ring-down spectrometer (OFFS-CRDS) to further enhance the intracavity power.[19] Doppler-free Lamb-dips were measured with kHz accuracy on ten lines of the 30013 ← 00001 band and two lines of the 31113 ← 01101 hot band of $^{12}C^{16}O_2$ near 1.6 μm, among the weakest ever studied by saturation spectroscopy (line intensity as weak as 5×10^{-25} cm/molecule[20]). More recently, Gatti *et al.*[21] used a comb-locked Lamb-dip spectrometer to determine the centers of three strong lines of acetylene near 1.54 μm with 2 kHz accuracy. Those lines have previously been measured by Madej *et al.*[22] A Lamb dip center accuracy on the same order (a few kHz) was achieved by Twagirayezu *et al.* for more than 130 relatively weak lines of the 10110-00010 and 10101-00001 hot bands of acetylene.[23]

a)Author to whom correspondence should be addressed: Alain.Campargue@univ-grenoble-alpes.fr

In addition of facilitating the line center determination, saturation spectroscopy allows for resolving highly blended lines. An attractive application of saturated CA-CRDS is the partial resolution of the hyperfine structure of the $^{17}O^{12}C^{16}O$ $R(0)$ fundamental transition near 2340 cm^{-1} and the measurement of the absolute frequencies of the hyperfine triplet with an accuracy of a few kHz.[24] In the present work, we use a modified version of the comb-assisted OFFS-CRDS setup developed by Burkart *et al.*[19] to accurately measure Doppler-free saturated-absorption Lamb dips of eight water lines near 7170 cm^{-1}. The targeted transitions were chosen to illustrate the advantages of the system in terms of both frequency accuracy and spectral resolution. Three highly blended K-type doublets with frequency separation of a few MHz are fully resolved while they appear as single lines in the Doppler regime. The 12 kHz frequency accuracy of the retrieved line centers allows discussing the quality of the line centers in the most commonly used spectroscopic database of water vapor. Furthermore, the three highly blended K-type doublets are used to discuss the accuracy of various recent high-quality *ab initio* water line lists.

II. EXPERIMENTAL

The present instrument combines an ultrasensitive cavity ring-down spectrometer and a very narrow, highly stable V-cavity-based optical feedback (VCOF) type light source.[24–26] The reader is referred to Refs. 19 and 25–27 for a detailed description of the first version of the experimental setup. The present OFFS-CRDS setup differs in different aspects from that applied to the measurement of saturated-absorption Lamb dips of CO_2 near 1.6 μm:[19] the working range is centered at 1.39 μm (215 THz), the VCOF source has been improved, it is faster and easier to operate, and its long-term reliability has been improved. In particular, the RD cavity is robustly dither-locked to the source rather than tight-lock using the Pound-Drever-Hall locking technique,[19] prone to frequent unlocking.

A. Laser source

The new VCOF reference cavity is made of a low expansion spacer, which has been machined and polished to be fitted with three mirrors by optical contact bonding. This source, hosting a DFB laser (Eblana Photonics), has sub-kHz emission line width, 10 mW output power, and exhibits a maximum frequency drift of 7 Hz/s. Its emission frequency is constantly monitored with both a wavemeter (HighFinesse, 20 MHz accuracy, 5 MHz resolution) and a GPS disciplined, self-referenced OFC (250 MHz repetition rate, −20 MHz carrier offset frequency) in order to determine its absolute optical emitting frequency with sub-kHz accuracy.[19] This frequency measurement was used in several of our previous studies.[8–10,19] It consists in refining the wavemeter readings by additionally measuring the beat note (BN) between the laser and the closest tooth of the OFC. The BN is recorded 100 times per second using a fast acquisition card (2^{15} samples recorded at 2.5×10^8 samples/s). A real time fast Fourier transform (FFT) of this signal is computed, leading to a 7.6 kHz resolution spectrum of which only the lowest frequency peak detected, i.e., in the 0-125 MHz range, determines the so-called BN frequency. The precision of this method is shown in Fig. 1 as an Allan deviation plot of a BN frequency series. It shows that the BN is determined within 42 kHz in a single shot (10 ms), and down to 700 Hz after 60 s averaging, which corresponds to a relative frequency determination of 2×10^{-10} and 3×10^{-12}, respectively. The GPS-disciplined rubidium clock driving the OFC electronics exhibits a noise excess at 2 s averaging. After about 80 s, the VCOF frequency drift is visible, which is accounted for in the frequency calibration process. According to the literature,[28] the present GPS referenced setup allows for absolute frequency determination with a relative accuracy better than 10^{-12}, i.e., 200 Hz. The wavemeter readings allow for a quasi-unambiguous determination of the OFC tooth index (N) beating with the VCOF, which frequency reads $\nu_{VCOF} = N \times 250 \pm BN - 20$ (MHz), where the sign is determined based on a determination of the relative position of the tooth frequency towards the VCOF frequency. In case of ambiguity, the sign can be explicitly deduced from the BN obtained by briefly locking the VCOF to an adjacent mode of its very stable reference cavity.

In OFFS-CRDS experiments,[19,26,27,29,30] the frequency tunability of the light source is obtained by adding or subtracting a radio frequency (RF) to the fixed laser frequency. A fibered I/Q modulator (iXblue) used as a single side band modulator (SSBM) is inserted in-between the VCOF and the CRD cell. It allows for fine and arbitrary tuning of the laser frequency within a range of ±2 to ±18 GHz, by applying clean GPS-referenced-RF (SMF100A, Rohde & Schwarz) and a series of static voltages to the modulator driving inputs. The SSBM efficiency is close to 10% and the carrier and other sidebands suppression ratio reaches 30 dB.

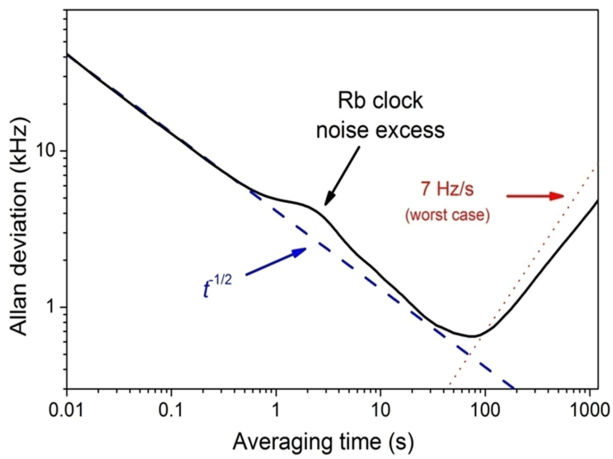

FIG. 1. Allan variance plot of a series of beat note measurements (black curve) recorded 100 times per second with 7.6 kHz FFT resolution (see the text). The single shot precision is 42 kHz, due to OFC noise. The precision reaches 700 Hz after 60 s averaging, closely following the ideal $t^{-1/2}$ random noise averaging (blue dashed curve). However, a noise excess is observed after 2 s averaging time and is attributed to noise excess in the rubidium reference clock driving the OFC electronics. After 80 s averaging, the VCOF frequency drift is clearly visible. The effect of a 7 Hz/s drift, which is the worst expected case, is plotted (red dotted line).

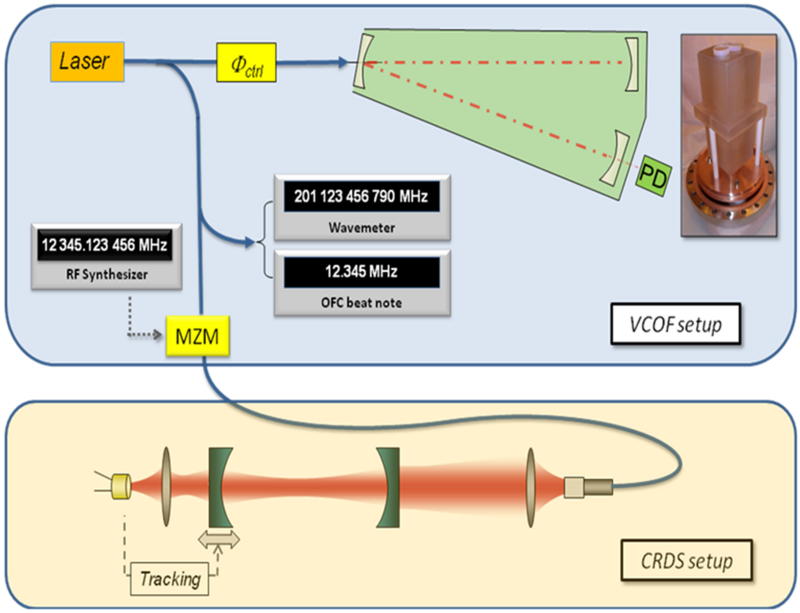

FIG. 2. Schematic of the experimental setup. A VCOF source is made from a laser that is locked by optical feedback to one chosen TEM_{00} mode of a V-shaped cavity made of three mirrors optically contacted on a precisely machined low-expansion material. The cavity is kept at constant temperature and under ultra-vacuum (see the picture in right inset). The relative phase between the laser and the cavity is precisely controlled (Φ_{ctrl}) by monitoring the cavity transmission and consequently acting on the laser-cavity distance. Its very stable emission frequency is accurately determined using both a precise Fizeau wavemeter and the BN obtained against a GPS-stabilized auto-referenced OFC. A Mach Zehnder modulator (MZM), configured as a single side band modulator (SSBM), allows the laser emission to be subsequently precisely tuned to an arbitrary wavelength by adding or subtracting a GPS-referenced radiofrequency in a range of 2-18 GHz. The shifted laser is used to sequentially probe the TEM_{00} modes of a massive CRDS cell, which are actively kept in resonance with the source using a dither-lock tracking scheme.

B. Ring down cavity

This precisely frequency shifted fully fibered laser carries about 1 mW power and is free-space coupled to a ring-down cell (Fig. 2). The mode matching is achieved with a single lens and two steering mirrors. In order to record ring-down events, the side band generation can be efficiently interrupted within 60 ns by switching the radio frequency off, using a high isolation fast PIN switch (>60 dB). A free space optical isolator is inserted between the two steering mirrors. The ring-down cell is made of a massive 30 cm long, 70 mm outer diameter, 13 mm inner diameter copper tube fitted with two highly reflective mirrors. One mirror is mounted on a piezoelectric tube actuator (10 nm/V expansion coefficient) so that the whole assembly forms a 32 cm long high finesse optical cavity (468 MHz FSR, F = 129 000). The two cavity mirrors can be precisely aligned by acting on two sets of 8 push- and pull-screws. The transmitted light is focused on a fast photo-detector (2 MHz band pass, 300 000 transimpedance gain) using a steering mirror and a lens. It allows for monitoring the cavity transmission and recording the ring-down events. To keep the setup simple and make the locking/relocking mechanism more robust, the cavity is dither-locked. Tracking electronics keep the cavity modes in coincidence with the laser by applying a 60 mV, 100 Hz triangular modulation on the mirror piezoactuator. With 44 μs maximal ring-down time and an excursion of about 400 kHz around the cavity modes, the Doppler effect associated with the cavity mirror displacement introduces a cavity mode frequency sweep of ±3.5 kHz per ring down, the sign being associated with the scan direction. Theoretically, the drift cancels out if one averages an even number of ring downs equally distributed amongst upward and backward scanning directions. Despite our efforts, a few spectral points may still be randomly biased by a fraction of ±5 kHz if a ring-down event was missed. However, given that the Lamb dip absorption features considered below are typically described by 40 spectral points, the dither-lock mechanism is expected to bias their center frequency to the sub-kHz level.

C. Saturated ring downs

Combining a very narrow laser and a stable high finesse cavity ensures an efficient laser-cavity coupling. Consequently, very high intracavity fields can be reached thanks to the intra-cavity electric-field buildup. The photodetector has a photosensitivity of 1 A/W and the transimpedance gain was set to 300 000. With a cavity finesse of $F \sim 129\,000$, corresponding to a mirror reflectivity of 99.9976%, assuming no additional losses and according to a beam waist of 400 μm, the intracavity power is calculated to be on the order of 25 W/cm^2 per V measured. The ring-downs are typically triggered at a threshold of 1.5 V, i.e., 40 W/cm^2. This value is 25 times lower than that used by Burkart *et al.*[19,25] to saturate CO_2 transitions, but the

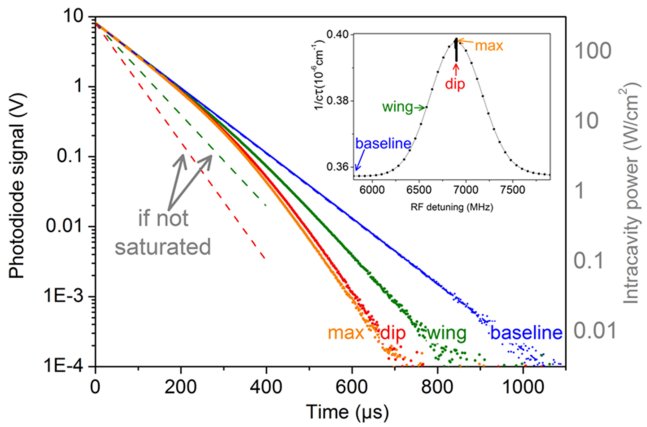

FIG. 3. Ring-down photodiode signals recorded on the baseline (blue dots), the wings (green dots), the maximum (orange dots), and dip center (red dots) of the water line doublet at 7185.596 cm^{-1}. Ring downs were acquired with a different CRDS cell (51 cm, F = 180 000). Each curve corresponds to an average of 1000 ring down events. The photodiode voltage (left scale) could be roughly converted to intracavity power (right scale) based on the mirror reflectivity and the photodetection chain gain. The green and red dashed lines indicate the saturation-free ring-down behavior expected on the wings (green) and on the top (red) of the absorption line, respectively. Effect of induced transparency is obvious within the first 100 μs of the event where intracavity power is in excess of 10 W/cm^2.

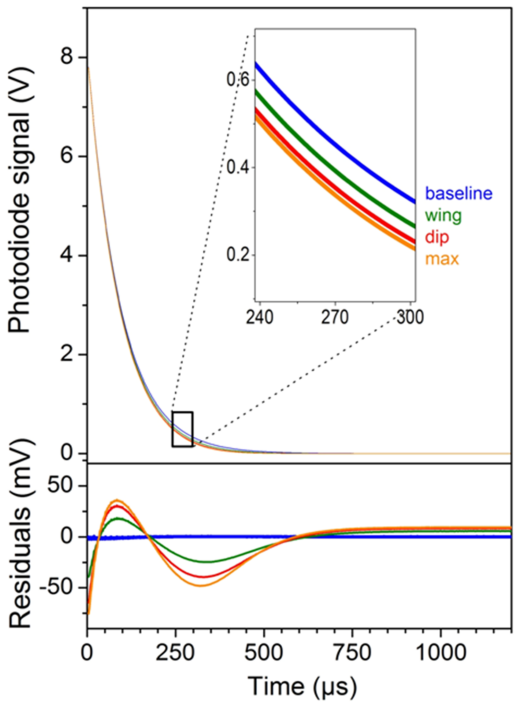

FIG. 4. Ring-down signal (upper panel) and corresponding exponential fit residuals (lower panel) observed at different spectral points of the line profile (see the inset of Fig. 3): baseline (blue), wings (green), dip center (red), and close to the maximum (orange) of the $\nu_1 + \nu_3$ [$6_{6\,0} \leftarrow 6_{61}$, $6_{61} \leftarrow 6_{60}$] line at 7185.596 cm^{-1}. Deviation to standard exponential (lower panel) increases with absorption. In the region of the dip, smaller residuals are observed as expected from a longer pseudo transparent regime induced by the higher effective incident optical power seen by zero z-axis velocity molecular class.

water transitions probed here have an Einstein coefficient that is three orders of magnitude higher.[20] To the best of our knowledge, none of the previous studies has reported CRDS Lamb dip measurement at such level of saturation. This is illustrated in Fig. 3 where the photodiode signal (in logarithm scale) is plotted *versus* time for three spectral points located out of the line profile, at about half width and near the line center. In the non-saturated regime, the light intensity decreases according to the cavity loss rate, $1/\tau_0 + \alpha(\nu)c$, which obviously varies over the frequency range of the line profile. This is not the case in the present recordings: The RD at the line center starts with a time constant close to that of the empty cavity. In other words, the saturation is so high that at the beginning of the RD, the gas appears to be transparent, over its whole line profile. The absorption line leads to an increase of the loss rate only after about 100 μs when the intracavity power has been decreased by about a factor of 10.

Let us highlight, that in a two-mirror optical cavity configuration, the TEM_{00} resonant mode is made of two contra-propagative optical waves perfectly overlapping each other. Optical cavities are thus an ideal tool to observe the Lamb dip feature that appears at the absorption line center, due to the twofold optical power experienced by molecules having zero velocity along the optical axis.[11–13] Because the present study is focused on accurate position measurement and not on a quantitative transition strength evaluation, we did not implement a non-exponential fit of the ring-down events that would explicitly take saturation into account.[24,29] The ring-down events were simply fitted with an exponential, therefore leading to strongly non-flat residuals (Fig. 4). Nevertheless, line profiles exhibit a well-marked Lamb dip feature at their center, with up to 14% contrast allowing for a precise line center determination.

D. Lamb dip recordings and center accuracy

Every line spectrum was acquired within 60 s including two successive passes: (i) A low resolution scan (2 GHz at 50 MHz resolution) used to roughly determine the line center from a simple Gaussian fit since pressure effects are negligible, (ii) a high resolution scan (4–40 MHz wide with 25 kHz resolution) around the determined center, where the Lamb dip features are expected. It results in a two-resolution spectrum, as shown in Fig. 5.

The dip center is retrieved by fitting the dip absorption using a Lorentzian function (see the inset of Fig. 5). The typical half-width at half-medium (HWHM) of the Lamb dip profile is 250 kHz. No evidence of asymmetry was found in the residuals. Therefore, albeit imperfect, the line fit model is expected to deliver unbiased line center determination.

In order to test the reproducibility of the experiment, we measured the $2\nu_1$ 1_{01}-1_{10} water line around 7182.2 cm^{-1} (215.5 THz) for several days. The RD cell was continuously pumped by a turbo-molecular pump, and outgasing water was probed at a residual pressure of less than 0.2 μbar. As depicted

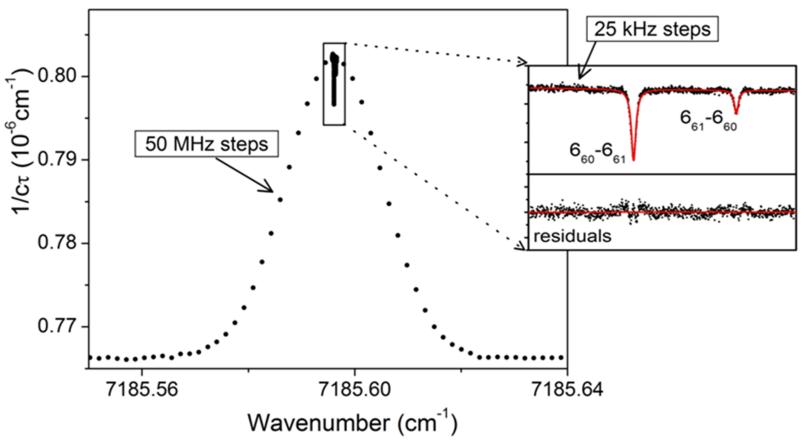

FIG. 5. Line profile and Lamb dip recordings with adaptive resolution. A first low resolution (50 MHz) survey scan is recorded, from which the line center is roughly determined using a Gaussian profile. The spectrum is immediately supplemented with a high resolution (25 kHz) scan around the center presented in the inset. The inset includes the residuals of the two observed Lamb dips using Lorentzian profiles leading to 1.5×10^{-10} cm^{-1} standard deviation of the residuals. No sign of profile asymmetry is observed.

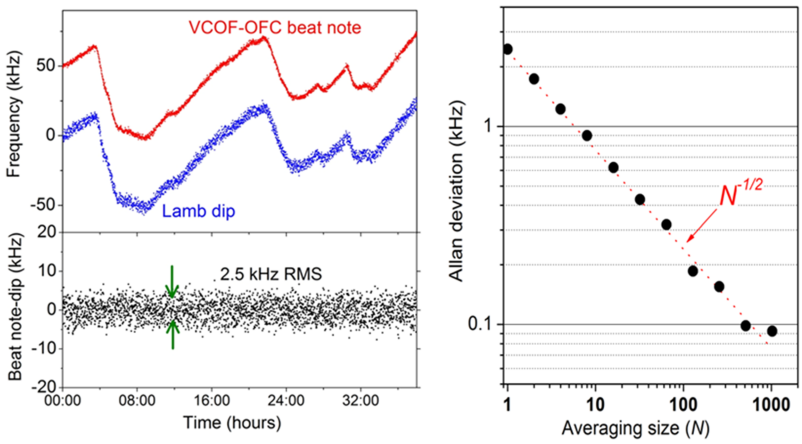

FIG. 6. The upper left panel shows a calibration free measurement series of a Lamb dip center. The blue curve corresponds to the evolution of the RF tuning frequency corresponding to the Lamb dip position. The red curve corresponds to the relative beat note between the VCOF and the GPS disciplined OFC, shifted up by 50 kHz on the plot for clarity. The difference is plotted (black dots) in the lower left panel revealing a perfect agreement with each other. The right panel is an Allan deviation plot of the difference. It shows first that a single Lamb dip position is determined with 2.5 kHz accuracy in a single scan and, second, that successive measurements average as $1/N^{1/2}$ and, third, that a precision better than 100 Hz is reached after averaging 500 measurements (about 8 h). This corresponds to a relative precision of 5×10^{-13} of the absolute Lamb dip position determination.

in Fig. 6, without OFC calibration, the apparent dip center is fluctuating over a 50 kHz range within two days. This drift is exclusively due to the imperfect stability of VCOF, as revealed by comparison with the BN monitoring, which exactly follows the same trend (red curve in Fig. 6). The (BN-dip) difference frequency is constant over time and shows 2.5 kHz RMS white noise, principally arising from the dip center fit precision. The Allan plot of this measurement series (Fig. 6) shows a quasi-perfect random noise type averaging behaviour, down to a statistical precision of 100 Hz, i.e., 5×10^{-13} relative to transition frequency. The self-pressure line shift, on the order of 300 kHz/Torr,[31] is expected to account for about 100 Hz, i.e., our measurement precision level. Because of the high symmetry of the experimental setup—two identical mirrors on a symmetry axis and laser off during the ring-down event—the geometry is not expected to induce frequency bias.[32] Thus, the main source of uncertainty remains the locking scheme even though we could not evidence it. Therefore, we indicate a conservative 1 kHz ($\sim 4 \times 10^{-8}$ cm^{-1}) accuracy for this line as an upper limit. A single scan was performed for each of the other lines, despite they are weaker and recorded at the same pressure. In view of their weakness and of the 2.5 kHz dispersion (7.5 kHz peak-to-peak) observed for the water line at 7182.2 cm^{-1}, we estimate their position to be determined with a conservative accuracy of 12 kHz ($\sim 4 \times 10^{-7}$ cm^{-1}) for a single scan.

III. RESULTS

Doppler-free saturated-absorption Lamb dips were measured at sub-Pa pressures on eight rovibrational lines of water near 7180 cm^{-1} (see Table I).

The measurements include three K-type doublets of $H_2{}^{16}O$ (see Fig. 7). Two doublets are the [$J_{J0} \leftarrow J_{J1}$, $J_{J1} \leftarrow J_{J0}$] doublets of the $\nu_1 + \nu_3$ band with $J = 6$ and 7. The ½ nuclear spin of hydrogen leads to a total nuclear spin of 0 and 1 corresponding to para- and ortho-water, respectively. Transitions are observed either between para or between ortho levels. Para and ortho energy levels in water can be classified according to the parity of the quantity $(K_a + K_c + V_3)$. Then, a $J_{J0} \leftarrow J_{J1}$ and $J_{J1} \leftarrow J_{J0}$ doublet involves a transition between para-energy levels and a transition between ortho-energy levels, the latter being three times stronger due to the spin statistics (ortho levels have a degeneracy of 3, while para levels are not degenerate). More precisely, for cold bands ($V_3 = 0$), the $J_{J1} \leftarrow J_{J0}$ component is the strongest when J is odd and the weakest when J is even. Thus, for the two studied doublets, the $7_{71} \leftarrow 7_{70}$ and $6_{60} \leftarrow 6_{61}$ dips are the strongest. Considering the close degeneracy of the two components, the relative intensity is the only criterion to discriminate the transitions corresponding to the two dips. We have included in Table I, the relative intensity of the studied doublets obtained from a Lorentzian fit of the dip profiles together with the

TABLE I. Assignments, HITRAN line parameters, and Lamb dip measurements of the eight studied water transitions near 1.39 μm.

			HITRAN2012[20]			Lamb dip		
Line number	Band	$JK'_aK'_c - JK''_aK''_c$	Wavenumber (cm^{-1})	Intensity (cm/molecule)	A (s^{-1})	Wavenumber (cm^{-1})	Int. ratio	Rel. dip depth (%)
1	$\nu_1+\nu_3$	7 7 1 7 7 0	7164.901 813(1000)	1.095×10^{-22}	14.50	7164.901 299 944(400)	3.02	13.9
2	$\nu_1+\nu_3$	7 7 0 7 7 1	7164.901 991(1000)	3.650×10^{-23}	14.50	7164.900 447 727(400)		4.6
3	$2\nu_2+\nu_3$	8 5 4 7 5 3	7174.083 890(1000)	8.068×10^{-24}	0.56	7174.083 983 975(400)		6.2
4	$\nu_1+\nu_3$	7 6 2 7 6 1	7179.752 215(1000)	1.802×10^{-22}	10.06	7179.751 953 517(400)	3.00	15.1
5	$\nu_1+\nu_3$	7 6 1 7 6 2	7179.753 363(1000)	6.009×10^{-23}	10.06	7179.751 538 877(400)		5.0
6	$2\nu_1$	1 0 1 1 1 0	7182.209 110(30)	1.541×10^{-21}	1.43	7182.208 851 005(100)		15.0
7	$\nu_1+\nu_3$	6 6 1 6 6 0	7185.596 571(1000)	1.995×10^{-22}	16.80	7185.596 432 547(400)	3.28	4.5
8	$\nu_1+\nu_3$	6 6 0 6 6 1	7185.596 909(1000)	5.984×10^{-22}	16.80	7185.596 112 566(400)		14.6

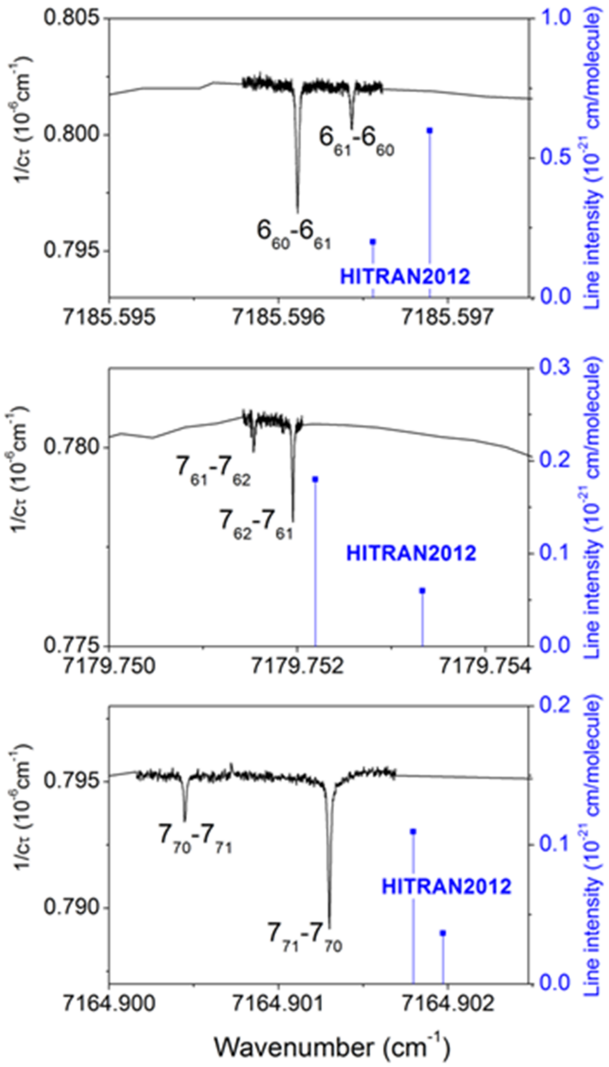

FIG. 7. Absorption line and Lamb dips for three K-type doublets of $H_2{}^{16}O$. On the lower panels, individual measurements points are showed to illustrate the higher resolution to sampling the dips range.

corresponding relative depth. The obtained intensity ratios are very close to 3.

Figure 8 presents the expected appearance of the $J_{J0} \leftarrow J_{J1}$ and $J_{J1} \leftarrow J_{J0}$ doublets in the absence of perturbation. The separation between the J_{J0} and J_{J1} energy levels decreases sharply with J. As the unperturbed J_{J0} energy level is higher than the J_{J1} level, the $J_{J1} \leftarrow J_{J0}$ transition is always observed at lower frequency. In the $J_{J0} \leftarrow J_{J1}$ and $J_{J1} \leftarrow J_{J0}$ series of doublets of the $\nu_1 + \nu_3$ band of $H_2{}^{16}O$, only the J = 1-4 doublets have been resolved (in the Doppler regime) and the measured frequency splittings were found to decrease from +10.47 cm^{-1} down to +0.106 cm^{-1}.[33] For comparison, the presently measured splittings are -2.9×10^{-4} and -8.5×10^{-4} cm^{-1}, for J = 6 and J = 7, respectively. We note that the sign of the J = 6 and 7 splittings is opposite to that of the $J \leq 4$ doublets and the relative position of the two components is inverted compared to the unperturbed case. In addition, the amplitude of the frequency splitting is larger for J = 7 than for J = 6. This situation is attributed to small perturbations of the considered energy levels of the (101) upper vibrational state, the (101) state being involved in the strong and complex interaction scheme of the first hexade of water {(040), (120), (200), (002), (021), (101)}.[34]

The Lamb dips of the $7_{6\,1} \leftarrow 7_{6\,2}$ and $7_{6\,2} \leftarrow 7_{6\,1}$ doublet were also resolved and assigned according to the relative intensity of the two components (Fig. 7).

IV. LINE POSITION ACCURACY OF WATER SPECTROSCOPIC DATABASES

A. Experimental and empirical databases

The eight $H_2{}^{16}O$ dip positions measured with 12 kHz accuracy (4×10^{-7} cm^{-1}) provide an accurate set of data for comparison to various spectroscopic databases of water vapor. Figure 9 shows the overview of the deviations from our measured dip values. The different data sets considered for the comparison are as follows:

(i) line positions calculated using the energy levels recommended by an IUPAC task group (IUPAC-TG) from an exhaustive review and evaluation of rovibrational lines positions, energy levels, and assignments for all the main isotopologues of water.[33] By using the procedure and code MARVEL (Measured Active Rotational-Vibrational Energy Levels),[35] all the high-quality absorption or emission line positions available in the literature were used to determine and validate the energy levels together with their self-consistent uncertainties. MARVEL uses a reweighted inversion process to determine the uncertainties which are given at 2σ. The IUPAC-TG used several hundred transition wavenumbers to derive the upper energy levels of each of the eight $H_2{}^{16}O$ transitions measured in this work.[33] As a result, these levels are reported with the best

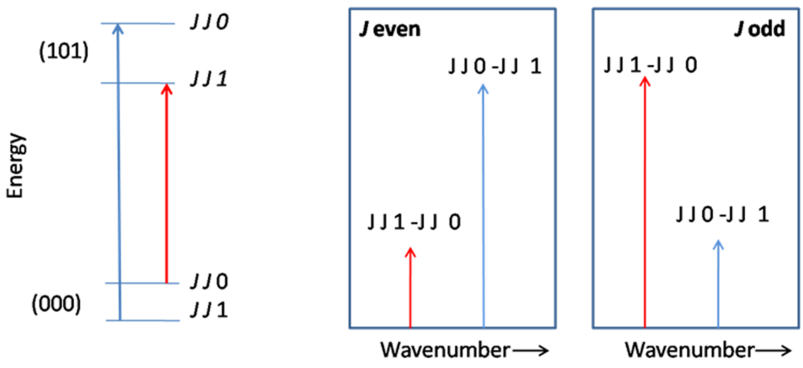

FIG. 8. Energy level scheme and relative intensity of the $J_{J0} \leftarrow J_{J1}$ and $J_{J1} \leftarrow J_{J0}$ doublets in water, according to the J parity.

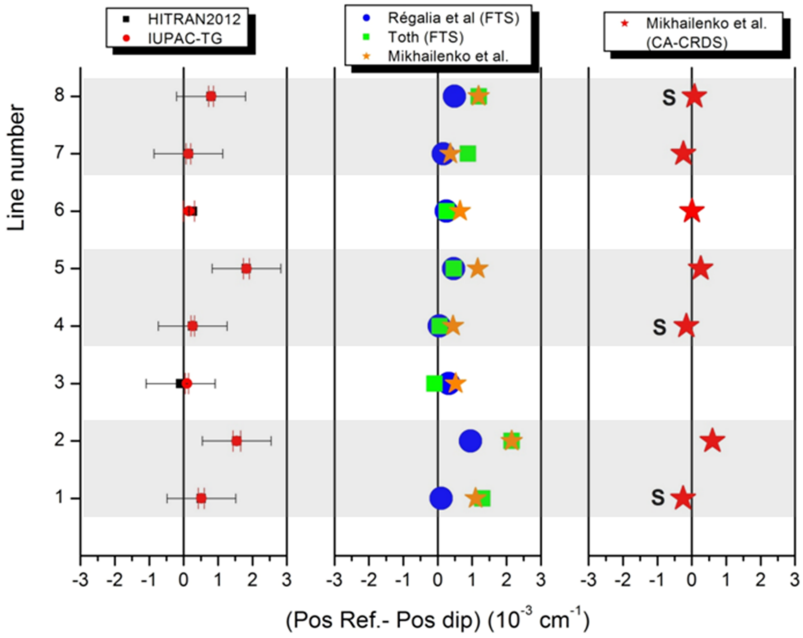

FIG. 9. Differences of the line positions to the dip center for the eight water lines measured near 7170 cm^{-1}. (The ranking number in the ordinate is the line number given in Table I.) The light grey zones indicate the three *K*-type doublets. From left to right, the comparison applies to HITRAN2012[20] and IUPAC-TG line positions[33] (left panel), FTS values by Toth[36] and Régalia *et al.*[37] and empirical values of Ref. 39 (center panel), and the recently obtained position values measured by CA-CRDS in the Doppler regime[44] (right panel, the **S** symbol indicates the strongest of the doublet components).

quality grade in the IUPAC-TG gradation (A+) and their uncertainty values (included in Fig. 9) range from 10^{-9} (!) to 3×10^{-5} cm^{-1}. The IUPAC-TG line positions are observed to deviate from our measurements by much larger values, up to 1.8×10^{-3} cm^{-1}. In our opinion, the main reason of this strong disagreement is that the considered IUPAC-TG energy levels have an uncertainty which is underestimated by several orders of magnitude. This may be due to underestimated error bars provided by some of the sources used by MARVEL or to some problems with the inversion process. In particular, the three *K*-type $H_2{}^{16}O$ doublets were resolved in neither experimental source used by the IUPAC-TG and the error bar of the upper levels cannot be smaller than the doublet reparation;

(ii) line positions retrieved in the Doppler regime from Fourier transform spectra recorded by Toth[36] and Régalia *et al.*;[37]

(iii) the HITRAN spectroscopic database[17] which uses different sources for the considered transitions. Six transitions have frequencies calculated from the IUPAC-TG levels, the two others being experimental values by Toth[36] and Jenouvrier *et al.*[38] The error code (4) is attached to all but one HITRAN2012 positions and corresponds to an uncertainty better than 10^{-3} cm^{-1}. This value is much larger than the corresponding IUPAC-TG error bars. We have included in Figs. 7 and 9, the HITRAN stick spectrum for the three studied *K*-type doublets. In the three cases, the frequency ordering of the ortho- and para- components is inverted compared to the observations. Nevertheless, the HITRAN2012 and dip position values are mostly consistent within the 10^{-3} cm^{-1} HITRAN error bar, the largest discrepancies concerning the weakest component of two *K*-type doublets;

(iv) transition frequencies provided in the near infrared spectroscopic database constructed by Mikhailenko *et al.*[40] The frequency values were obtained from empirically determined energy values mostly based on extensive investigations of water spectra by high sensitivity CRDS[41–43] complemented with literature data (in particular the FTS data by Toth[33] and Régalia *et al.*[34]);

(v) $H_2{}^{16}O$ line positions measured in the Doppler regime at low pressure (<0.2 Torr) by CA-CRDS of water highly enriched in ^{17}O.[44]

It is worth underlining that in the case of the three *K*-type doublets (light grey zones in Fig. 9), the three experimental studies in the Doppler regime by FTS[36,37] and CA-CRDS[44] provide a single line position for the two components. As expected, for the three *K*-type doublets, the reported line position is closer to the dip center of the strongest component. Interestingly, the CA-CRDS values[44] are intermediate between the two dip centers, and the amplitude of the deviation of the weaker dip is not far from three times that of the stronger dip, as expected from their relative intensity. Two factors contribute to the higher accuracy of the CA-CRDS values: the referencing of the laser source to the optical frequency comb and the higher sensitivity of the CRDS technique allowing for measurements at very low pressure.

B. Variational line lists

High-quality-computed water line lists are available since two decades. Since the pioneer studies by Partridge and Schwenke,[45,46] the collaboration between University College London and the Institute of Applied Physics in Nizhny Novgorod has produced various line lists based on different versions of the potential energy and dipole moment surfaces.[47–50] They differ in terms of accuracy and completeness (maximum energy of the levels, maximum *J* values). In Table II, we compare the line positions of the three $H_2{}^{16}O$ *K*-type doublets to the computed values of five variational calculations, from the

TABLE II. Comparison of the Lamb dip centers of the three measured K-type doublets to the predictions of various variational calculations.

			Variational-dip (10^{-3} cm^{-1})					Doublet separation (10^{-3} cm^{-1})					
Band	$JK'_aK'_c - JK''_aK''_c$	Lamb dip center (cm^{-1})	Pokazatel[47]	Reference 48	Reference 49	BT2[50]	SP[45,51]	Lamb dip	Pokazatel[47]	Reference 48	Reference 49	BT2[50]	SP[45,51]	HITRAN2012[20]
$\nu_1+\nu_3$	7 7 1 7 7 0	7164.901 299 944(400)	−34.70	−10.08	917.41	96.70	−33.49	−0.8522	−0.858	−0.847	−0.852	−0.8	−0.92	+0.178
$\nu_1+\nu_3$	7 7 0 7 7 1	7164.900 447 727(400)	−34.71	−10.07	917.41	96.75	−33.56							
$\nu_1+\nu_3$	7 6 2 7 6 1	7179.751 953 517(400)	−47.31	−5.38	650.3	104.05	−9.59	−0.4146	−0.440	−0.316	+1.682	−0.6	0.00	+1.15
$\nu_1+\nu_3$	7 6 1 7 6 2	7179.751 538 877(400)	−47.34	−5.28	652.4	103.86	−9.18							
$\nu_1+\nu_3$	6 6 1 6 6 0	7185.596 432 547(400)	0.80	−16.78	936.85	68.57	−14.45	−0.3200	−0.332	−0.313	−0.318	−0.4	+0.51	+0.338
$\nu_1+\nu_3$	6 6 0 6 6 1	7185.596 112 566(400)	0.79	−16.78	936.86	68.59	−13.62							

list released by Schwenke and Partridge (SP) in 1997 up to the very recent POKAZATEL list by Polyansky *et al.*[47] For SP values, we used the values computed by Tashkun, available in Ref. 51. In terms of absolute position values, no clear improvement is noted for the three considered doublets, the deviations being in the 0.01-0.10 cm^{-1} range except for Ref. 49 for which larger differences are noted (contrary to the others, the values of Ref. 49 are pure *ab initio* values without any experimental corrections). However, the improvement is obvious for the K-type doublet separations. While SP separations show large differences including for the sign, the POKAZATEL separations show an impressive agreement with the measured values, at the 10^{-5} cm^{-1} level. It would be interesting to trace the origin of such achievement in order to identify which family of levels has energies predicted with such high *relative* accuracy.

V. CONCLUSION

An ultrasensitive cavity ring-down spectrometer injected by a very narrow, highly stable V-cavity-based optical feedback type light source[25] has been developed for accurate spectroscopy in the near infrared.[24–26] The V-shaped optical feedback source (VCOF) provides a sub-kHz laser linewidth with a very high stability (typical drift of 10 Hz/s) which makes the setup particularly suitable for line shape studies and precise measurements of isotopologue abundances.[30] Very high intracavity fields are obtained by this combination of a very narrow laser and a stable high finesse cavity. In the present OFFS-CRDS setup, the obtained intracavity power (about 40 W/cm^2) was used to induce a high saturation of strong rovibrational lines of water vapor (Einstein coefficient in the 1-10 s^{-1} range). At the ring-down starting point, the intracavity power was roughly estimated to be 10 times higher than the saturation intensity. Therefore, an almost completely induced transparency regime was reached so that at the early stage of the ring down, the decay time is identical to that of the empty cavity. By referencing the laser source, the developed setup allows determining line centers of highly K-type blended doublets from their much narrower Lamb dip signatures, having 250 kHz HWHM. As the component separation is about 10 MHz to be compared to a HWHM Doppler width on the order of 300 MHz, our measurements contrast with previous experimental studies where the doublets were observed as single lines. The chosen examples illustrate the advantage of Lamb dip spectroscopy for accurate measurement of line centers. In the Doppler regime, line center determination with kHz accuracy requires a precise modeling of the full line profile and the absence of interfering line with a very high contrast, while in Lamb dip spectroscopy, these requirements are much relaxed. In particular, we demonstrate that averaging measurement series allows for line position to be statistically determined to 100 Hz precision, i.e., to the remarkable 5×10^{-13} relative precision.

The obtained position measurements have been discussed in relation with widely used water line lists. In particular, the error bars provided by the IUPAC-TG for the energy levels involved have been found considerably underestimated. The comparison to variational line lists indicates that absolute

positions deviate from the measurements by 0.01-0.1 cm^{-1} for all the considered lists, but the recent POKAZATEL list[47] provides an impressive agreement at the 10^{-5} cm^{-1} level, for the three studied K-type doublets splitting.

ACKNOWLEDGMENTS

This work was supported by the Agence Nationale de la Recherche (Grant No. ANR-13-JS060005), INSU-CNRS (LEFE/ChAt) and Labex OSUG@2020 (Grant No. ANR10 LABX56). We are grateful to the Université Joseph Fourier and the GRAM Equipex REFIMEVE+ for additional financial support. M.C. has received funding from the European Research Council under the European Union's Seventh Framework Programme (Grant No. FP7/2007-2013)/RC, Grant Agreement No. 306045, attributed to A. Landais (LSCE) to whom we are very indebted, since this grant is also highly contributed to the experimental developments of the present setup, dedicated to ultra-precise water spectroscopy. We thank A. A. Kyuberis and O. L. Polyansky (Institute of Applied Physics in Nizhny Novgorod) for providing us with unpublished variational position values included in Table II. We are indebted to S. N. Mikhailenko (Institute of Atmospheric Optics, Tomsk) for valuable discussion and information about the K-type splitting in water.

[1] T. Udem, R. Holzwarth, and T. W. Hänsch, Nature **416**, 233–237 (2002).
[2] D. Long, G.-W. Truong, J. Hodges, and C. Miller, J. Quant. Spectrosc. Radiat. Transfer **130**, 112–115 (2013).
[3] K. K. Bielska, S. Wójtewicz, P. Morzynski, P. Ablewski, A. Cygan, M. Bober, J. Domysławska, M. Zawada, R. Ciuryło, P. Masłowski, and D. Lisak, J. Quant. Spectrosc. Radiat. Transfer **201**, 156–160 (2017).
[4] V. T. Sironneau and J. T. Hodges, J. Quant. Spectrosc. Radiat. Transfer **152**, 1–15 (2015).
[5] J. Domysławska, S. Wójtewicz, D. Lisak, A. Cygan, F. Ozimek, K. Stec *et al.*, J. Chem. Phys. **136**, 024201 (2012).
[6] M. Zolot, F. R. Giorgetta, E. Baumann, W. C. Swann, I. Coddington, and N. R. Newbury, J. Quant. Spectrosc. Radiat. Transfer **118**, 26–39 (2013).
[7] D. Mazzotti, P. Cancio, A. Castrillo, I. Galli, G. Giusfredi, and P. De Natale, J. Opt. A: Pure Appl. Opt. **8**, S490–S493 (2006).
[8] D. Mondelain, T. Sala, S. Kassi, D. Romanini, M. Marangoni, and A. Campargue, J. Quant. Spectrosc. Radiat. Transfer **154**, 35–43 (2015).
[9] D. Mondelain, S. N. Mikhailenko, E. V. Karlovets, S. Béguier, S. Kassi, and A. Campargue, J. Quant. Spectrosc. Radiat. Transfer **203**, 206 (2017).
[10] D. Mondelain, S. Kassi, T. Sala, D. Romanini, M. Marangoni, and A. Campargue, J. Mol. Spectrosc. **326**, 5–8 (2016).
[11] T. Hänsch, I. Shahin, and A. Schawlow, Nature **235**, 63–65 (1972).
[12] D. Romanini, P. Dupré, and R. Jost, Vib. Spectrosc. **19**, 93–106 (1999).
[13] C. R. Bucher, K. K. Lehmann, D. F. Plusquellic, and G. T. Fraser, Appl. Opt. **39**, 3154–3164 (2000).
[14] G. Gagliardi, G. Rusciano, and L. Gianfrani, Appl. Phys. B **70**, 883–888 (2000).
[15] I. Galli, S. Bartalini, P. Cancio Pastor, F. Cappelli, G. Giusfredi, D. Mazzotti, N. Akikusa, M. Yamanishi, and P. De Natale, Mol. Phys. **111**, 2041–2045 (2013).
[16] D. Lisak and J. T. Hodges, Appl. Phys. B **88**, 317–325 (2007).
[17] G. Galzerano, E. Fasci, A. Castrillo, A. Coluccelli, L. Gianfrani, and P. Laporta, Opt. Lett. **34**, 3107–3110 (2009).
[18] G. Galzerano, A. Gambetta, E. Fasci, A. Castrillo, M. Marangoni, P. Laporta *et al.*, Appl. Phys. B **102**, 725–729 (2010).
[19] J. Burkart, T. Sala, D. Romanini, M. Marangoni, A. Campargue, and S. Kassi, J. Chem. Phys. **142**, 191103 (2015).
[20] L. S. Rothman, I. E. Gordon, Y. Babikov, A. Barbe, D. Chris Benner, P. F. Bernath, M. Birk, L. Bizzocchi, V. Boudon, L. R. Brown, A. Campargue, K. Chance, L. Coudert, V. M. Devi, B. J. Drouin, A. Fayt, J.-M. Flaud, R. R. Gamache, J. Harrison, J.-M. Hartmann, C. Hill, J. T. Hodges, D. Jacquemart, A. Jolly, J. Lamouroux, R. J. LeRoy, G. Lia, D. Longo, C. J. Mackie, S. T. Massie, S. Mikhailenko, H. S. P. Müller, O. V. Naumenko, A. V. Nikitin, J. Orphal, V. Perevalov, A. Perrin, E. R. Polovtseva, C. Richard, M. A. H. Smith, E. Starikova, K. Sung, S. Tashkun, J. Tennyson, G. C. Toon, Vl. G. Tyuterev, J. Vander Auwera, and G. Wagner, J. Quant. Spectrosc. Radiat. Transfer **130**, 4–50 (2013).
[21] D. Gatti, R. Gotti, A. Gambetta, M. Belmonte, G. Galzerano, P. Laporta *et al.*, Sci. Rep. **6**, 27183 (2016).
[22] A. Madej, A. J. Alcock, A. Czajkowski, J. E. Bernard, and S. Chepurov, J. Opt. Soc. Am. B **23**, 2200–2208 (2006).
[23] S. Twagirayezu, M. J. Cich, T. J. Sears, C. P. McRaven, and G. E. Hall, J. Mol. Spectrosc. **316**, 64–71 (2015).
[24] G. Giusfredi, S. Bartalini, S. Borri, P. Cancio, I. Galli, D. Mazzotti, and P. De Natale, Phys. Rev. Lett. **104**, 110801 (2010).
[25] J. Burkart, D. Romanini, and S. Kassi, Opt. Lett. **38**, 2062–2064 (2013).
[26] J. Burkart, D. Romanini, and S. Kassi, Opt. Lett. **39**, 4695–4698 (2014).
[27] J. Burkart and S. Kassi, Appl. Phys. B **119**, 97–109 (2015).
[28] J. A. Stone and P. Egan, J. Res. Natl. Inst. Stand. Technol. **115**, 413–431 (2010).
[29] J. Burkart, Ph.D. thesis, Université Joseph Fourier de Grenoble, 2015.
[30] T. Stoltmann, M. Casado, M. Daëron, A. Landais, and S. Kassi, Anal. Chem. **89**, 10129 (2017).
[31] B. E. Grossman and E. V. Browell, J. Mol. Spectrosc. **136**, 264–294 (1989).
[32] C. J. Bordé, J. L. Hall, C. V. Kunasz, and D. G. Hummer, Phys. Rev. A **14**(1), 236–263 (1976).
[33] J. Tennyson, P. F. Bernath, L. R. Brown, A. Campargue, A. G. Császár, L. Daumont, R. R. Gamache, J. T. Hodges, O. V. Naumenko, O. L. Polyansky, L. S. Rothman, A. C. Vandaele, N. F. Zobov, A. R. Al Derzi, A. Z. Fazliev, T. Furtenbacher, I. F. Gordon, and L. Lodi, J. Quant. Spectrosc. Radiat. Transfer **117**, 29–58 (2013).
[34] V. I. Starikov and S. N. Mikhailenko, J. Mol. Struct. **442**, 39–53 (1998).
[35] T. Furtenbacher, A. Csaszar, and J. Tennyson, J. Mol. Spectrosc. **245**, 115–125 (2007).
[36] R. A. Toth, Appl. Opt. **33**, 4868–4879 (1994).
[37] L. Régalia, C. Oudot, S. Mikhailenko, L. Wang, X. Thomas, A. Jenouvrier, and P. Von der Heyden, J. Quant. Spectrosc. Radiat. Transfer **136**, 119–136 (2014).
[38] A. Jenouvrier, L. Daumont, L. Régalia-Jarlot, Vl. G. Tyuterev, M. Carleer, A. C. Vandaele, S. Mikhailenko, and S. Fally, J. Quant. Spectrosc. Radiat. Transfer **105**, 326–355 (2007).
[39] S. N. Mikhailenko, S. Kassi, D. Mondelain, R. R. Gamache, and A. Campargue, J. Quant. Spectrosc. Radiat. Transfer **179**, 198–216 (2016).
[40] S. Mikhailenko, S. Kassi, L. Wang, and A. Campargue, J. Mol. Spectrosc. **269**, 92–103 (2011).
[41] O. Leshchishina, S. Mikhailenko, D. Mondelain, S. Kassi, and A. Campargue, J. Quant. Spectrosc. Radiat. Transfer **113**, 2155–2166 (2012).
[42] O. Leshchishina, S. Mikhailenko, D. Mondelain, S. Kassi, and A. Campargue, J. Quant. Spectrosc. Radiat. Transfer **130**, 69–80 (2013).
[43] S. N. Campargue, B. G. Mikhailenko, E. V. Lohan, D. Karlovets, Mondelain, and S. Kassi, J. Quant. Spectrosc. Radiat. Transfer **157**, 135–152 (2015).
[44] S. N. Mikhailenko, D. Mondelain, E. V. Karlovets, S. Kassi, and A. Campargue, J. Quant. Spectrosc. Radiat. Transfer **206**, 163–171 (2018).
[45] H. Partridge and D. W. Schwenke, J. Chem. Phys. **106**, 4618–4639 (1997).
[46] D. W. Schwenke and H. Partridge, J. Chem. Phys. **113**, 6592–6597 (2000).
[47] O. L. Polyansky, A. A. Kyuberis, N. F. Zobov, J. Tennyson, S. N. Yurchenko, and L. Lodi, private communication (October 2017).
[48] I. Bubukina, N. F. Zobov, O. L. Polyansky, S. V. Shirin, and S. N. Yurchenko, Opt. Spectrosc. **110**, 160–166 (2011).
[49] O. L. Polyansky, R. I. Ovsyannikov, A. A. Kyuberis, L. Lodi, J. Tennyson, and N. F. Zobov, J. Phys. Chem. **117**, 9633–9643 (2013).
[50] R. J. Barber, J. Tennyson, G. J. Harris, and R. N. Tolchenov, Mon. Not. R. Astron. Soc. **368**, 1087–1094 (2006).
[51] See http://spectra.iao.ru/1536x765/en/mol/survey/1/ for water line lists based on variational calculations by Schwenke and Partridge.